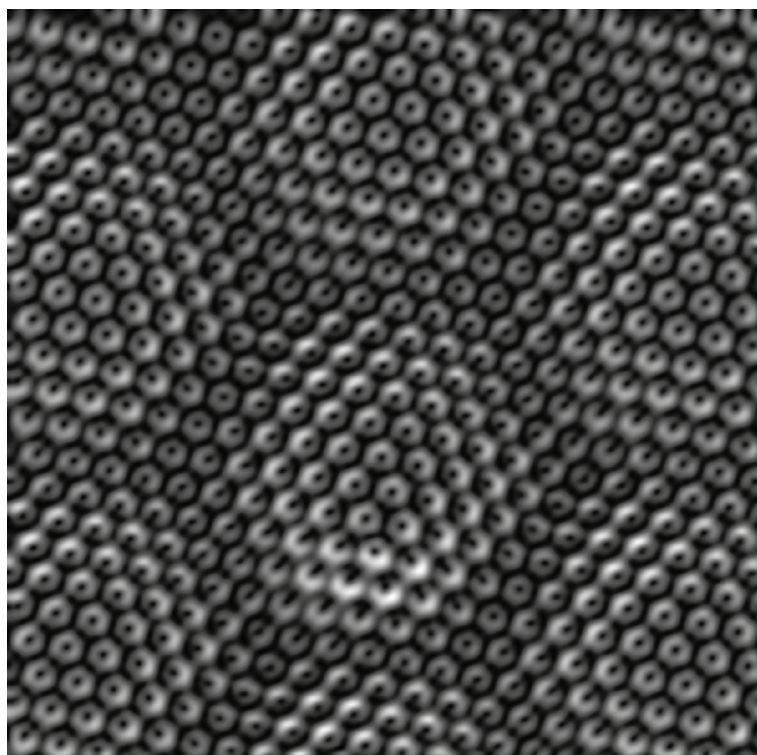




Universiteit Utrecht

MASTER THESIS

Chemical identification by AFM: A tool to study N-doped graphene



Written by

Daniël Smith, B. Sc.

Supervised by

Nadine van der Heijden, M. Sc.

Dr. Ingmar Swart

2014-2016

Condensed Matter and Interfaces
Debye Institute for Nanomaterials Science
UTRECHT UNIVERSITY

Abstract

The properties of single dopants in doped graphene are of crucial importance for an understanding of the material properties. In this thesis we present chemical identification by AFM as a tool for the study of these dopants in N-doped graphene. The observed results in this thesis were compared to DFT calculations which were in excellent agreement with each other. Chemical identification was successfully applied to single graphitic N-dopants in N-doped graphene on Cu(111). The obtained $df(z)$ -spectra and df -maps clearly show a more negative value in the minimum of the $df(z)$ curves for the N atom than for C atoms. Besides a Cu(111) substrate, N-doped graphene was also investigated on Ir(111). In this fashion, the effect of the modulated graphene-iridium interaction on chemical identification could be investigated. Since the different atoms in the Moiré cell have a different interaction with the substrate, measuring the N-dopant at different positions in the cell gives information on this effect. Lastly, possible candidates for double dopants were investigated which showed similar results to the measurements done on single dopants.

Contents

1	Introduction	7
1.1	Nanomaterials	7
1.2	Characterization of nanomaterials	8
1.3	Scope of this thesis	8
2	Theory	9
2.1	Scanning Probe Microscopy	9
2.1.1	Scanning Tunneling Microscopy	9
2.1.2	Atomic Force Microscopy	10
2.1.3	Chemical identification	12
2.2	Graphene	13
2.2.1	Synthesis of (doped) graphene	14
2.2.2	Graphene on a substrate	14
3	Experimental section	17
3.1	Graphene synthesis	17
3.2	Scanning Probe Measurements	19
3.2.1	Chemical identification	20
3.2.2	The strategy	20
4	Results and discussion	21
4.1	N-doped graphene on Cu(111)	21
4.1.1	Mapping a single dopant	23
4.2	N-doped graphene on Ir(111)	24
4.2.1	Chemically identifying single dopants	25
4.2.2	Double dopants?	26
5	Conclusions and outlook	29
	Acknowledgements	31
	Bibliography	33
	Appendices	35
	Appendix A Positions in the Moiré unit cell	37
	Appendix B Results of a different N-dopant on Cu(111)	39
	Appendix C Chemical identification according to DFT	41

Chapter 1

Introduction

Starting in the mid 1990's the first mentions of nanomaterials, nanoscience and nanotechnology popped up in literature.¹ In the following years there has been a steady increase in popularity in the field of nanoscience. Although nanoscience really took off only in these last decades, the first example of nanoscience (colloidal gold nanoparticles) was already described in 1857 by Faraday [1]. Although at the time he didn't know he was studying nanoparticles. It took the field of nanoscience some 150 years to advance from these first steps to expand into an extensive research direction.

The range of potential applications of nanoscience and nanomaterials is quite staggering. Examples are photovoltaics [2], catalysis [3], nanoelectronics [4] and biomedics [5] to name a few. Besides these applications, nanoscience is also interesting for the fundamental scientist. Matter at the nanoscale exhibits unique behaviours which sheds new light on physical phenomena [5]. There is still a lot left to explore. Or as the famous physicist Richard Feynman put it: there is plenty of room at the bottom. [6]

1.1 Nanomaterials

A nanomaterial is a piece of matter which has one or more of its spatial dimensions in the nanoscale regime i.e. 1-1000 nm. In this size range the transition from molecular to bulk matter takes place. Depending on the size of the nanomaterial, the properties can be either more bulk or more molecular like or a combination of both. Due to the size dependence of the properties, the properties can be tuned by changing the material's spatial dimensions. This tunability opens doors to make the right type of material for the job.

Graphene

Graphene is a type of nanomaterial. It consists of a monolayer of carbon atoms arranged in a honeycomb crystal lattice. This specific arrangement of atoms leads to very interesting material properties. For instance, electrons in graphene behave like they have an effective mass of zero. These 'massless' electrons move at very high velocities [7]. Combine this with the mechanical properties of graphene and you have an ideal candidate for the use in a new generation of nanoelectronics.

Despite of these promising properties, there are still some issues which need to be resolved before graphene can be used on a large scale. One of these issues is the lack of bandgap in graphene [7]. Multiple solutions for this issue have been suggested like, decreasing one of the lateral dimensions of graphene to make so called graphene nanoribbons [8]. A different solution is the usage of a different building block for the honeycomb lattice. Examples are silicon or phosphorus to make silicene [9] or phosphorene [10].

Another solution to this problem is similar to what is a well known procedure in the regular semiconductor industry. For a long time have the electronic properties of semiconductors been altered by the controlled addition of impurity atoms, this practice is called doping. The workhorse of the the modern semiconductor industry, silicon, can be doped with for instance gallium or arsenic. Which results in p- or n-type doping respectively. Examples of possible dopants for graphene are boron (B) and nitrogen

¹Determined using the Web of Science database

(N). B- and N-doped graphene has been successfully synthesized in the past few years and their properties are now actively being investigated. How the B atoms and N atoms are bound to the graphene is not yet fully understood while this is of crucial importance to the material properties [11].

1.2 Characterization of nanomaterials

Due to the small size of nanomaterials, characterization is a challenge. Optical, electron and X-ray microscopy are imaging techniques which can be used for the study of nanomaterials [3, 12, 13]. These microscopy techniques make use of the interaction of photons or electrons with matter. Each technique allows one to gain different insights in the material. A completely different approach is the use of a sharp needle to perform microscopy. These so called Scanning Probe Microscopy (SPM) techniques are ideally suited for the study of (nearly) flat materials. SPM gives insight in the properties of the surfaces of these materials. Graphene is therefore ideally suited for study by SPM.

Scanning Probe Microscopy

A SPM uses a sharp needle to 'feel' a substrate of interest. The first SPM was developed in 1982 by Binnig and Rohrer at IBM Research in Zurich [14]. This first SPM, a Scanning Tunneling Microscope (STM), made use of the quantum tunneling effect to produce images with very high resolution. After the STM came the development of the Atomic Force Microscope (AFM) in 1986 [15]. In AFM the tip-substrate force is used for imaging. These first SPMs were mainly used for the study of metallic and semiconducting surfaces with very high resolution [16]. Advances in especially AFM have led to the first atomically resolved images of single organic molecules [17]. Since then, these high resolution images of molecules are being made on a regular basis all over the world [18].

1.3 Scope of this thesis

In the last couple of years an increasing interest has grown in the fundamental aspects of SPM. Important questions are: what are the causes of the contrast seen in AFM [19]? What are all the things an SPM can be used for [18, 20]? These questions lead to the scope of this thesis.

In AFM images all the atoms appear in more or less the same contrast. How can we distinguish between different types of atoms? First described by Sugimoto et al. is the process of chemical identification by Atomic Force Spectroscopy. They measured force-distance spectra on multiple atoms of a substrate. The obtained spectra closely resemble Lennard-Jones -or Morse-like potentials. It was found that this technique allows for the differentiation between elements (Si, Pb and Sn atoms) of a semiconducting surface [20]. This technique was later extended to organic systems by van der Heijden et al. [21]. They managed to differentiate between a N atom and C atoms in a single molecule. In this thesis it is explored if this technique can be applied to N-doped graphene. We want to see if chemical identification by AFM could be a tool in the study of individual N-dopants in graphene.

The graphene studied in this thesis is laying on a substrate. To see how the substrate affects the process of chemical identification the substrate is varied. The obtained results are compared with Density Functional Theory (DFT) calculations which have been done for graphene on Ir(111). Explaining the details of these calculations falls outside the scope of this thesis but some of the main results are included in appendix C. For an in depth description of these calculations the report of Calogero can be consulted [22].

Since doped graphene has been studied by STM extensively in the last decade it is well known how single N-dopants appear in STM images [23]. Therefore, we use STM measurements as a starting point in our research. After which we will do the chemical identification by AFM measurements.

Chapter 2

Theory

This chapter consists of two parts. The first part briefly describes the theory of Scanning Probe Microscopy (SPM), the analysis tool used in this research. This part highlights core concepts on the theory of Scanning Tunneling Microscopy (STM) and Atomic Force Microscopy (AFM) which are needed to understand why chemical identification works. The second section discusses the material of interest: graphene. General aspects of graphene, the synthesis and the influence of the substrate on the properties are mentioned.

2.1 Scanning Probe Microscopy

The main characteristic feature of SPM is the usage of a sharp tip which probes a surface of interest. When the tip is brought into close proximity to the substrate a number of physical phenomena start to play a role. Two of these effects are quantum tunneling of electrons and the tip-substrate force. If the the first effect is used for imaging, the SPM is called an STM and in the latter an AFM.

2.1.1 Scanning Tunneling Microscopy

In quantum mechanics particles can go through a potential energy barrier from one place to another. This effect, called tunneling, is the physical principle underlaying STM. In STM an atomically sharp tip is connected to a substrate in an electric circuit. An example of such a circuit is given in figure 2.1.

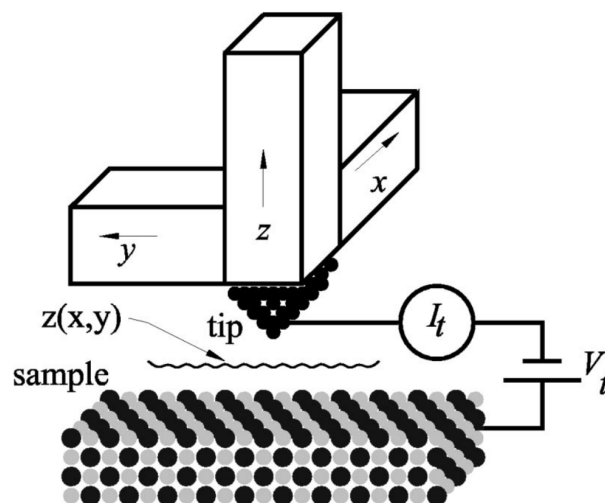


Figure 2.1: Electronic circuit used in STM. The xyz blocks are the piezoelectric elements used for controlling the tip, I_t measures the tunneling current and V_t denotes the applied potential. Image taken from ref. [24].

If the tip is close enough to the substrate and a bias voltage is applied on the tunneling junction, electrons start to tunnel. By changing this voltage, the Fermi level (E_f) of the tip can be changed.

By changing E_f , electrons can start to tunnel through different electronic states of the sample. In this fashion information on the electronic structure of the sample can be obtained.

There are two operating modes in STM: constant height and constant current. In constant height the tip is raster scanned over the surface at constant tip-substrate height. The tunneling current is recorded at every pixel and in such a way an 'image' of the surface is obtained. In constant current mode, a feedback loop keeps the tunneling current constant by adjusting the tip-substrate height recording a topological map of the surface. In equation 2.1 the relation between tunneling current (I) and the distance (d) can be seen.

$$I \propto e^{(-\kappa d)} \quad (2.1)$$

With $\kappa \sim 1\text{\AA}$ as proportionality constant. This exponential relation illustrates why STM is so sensitive for small height differences. For a more elaborate view of tunneling and STM the reader is encouraged to refer to ref. [25].

2.1.2 Atomic Force Microscopy

Since the first AFM was developed, the technique has grown into a versatile characterization tool. The versatility of AFM is due to the multiple ways AFM measurements can be done. Each variant has its own advantages and disadvantages which makes it useful for different experiments. It is outside the scope of this thesis to discuss every AFM technique there is. Some key concepts are discussed but for a more in depth analysis the interested reader can refer to ref. [24].

The fundamentals

AFM is based on the effect of what happens when two particles come close to each other. When the particles are far away there is little interaction. Due to van der Waals (vdW) interactions, particles will start to feel an attractive force when they come closer towards each other. When the particles are too close, Pauli repulsion dominates and the particles feel a repulsive force. This behavior is usually modeled with semi empirical equations such as for instance a Lennard-Jones potential (LJ) which is shown in eq 2.2.

$$V(r) = 4\epsilon\left(\left(\frac{\sigma}{r}\right)^{12} - \left(\frac{\sigma}{r}\right)^6\right) \quad (2.2)$$

With $V(r)$ the potential energy, ϵ the depth of well, σ the distance between two particles where their interaction is zero and r the distance between the two particles. Another well known potential is the Morse potential, eq 2.3.

$$V(r) = D_e(1 - e^{-\alpha(r-r_e)})^2 \quad (2.3)$$

With D_e the depth of well, r_e the position of the well, and α is related to the broadness of the well which is related to the spring constant in interatomic bonds. Morse and LJ potentials are very different mathematically, but they can be applied to the same physical phenomenon. Which potential one uses is therefore arbitrary and usually depends on things like computational cost or explanatory value. Since $F = \frac{\partial V}{\partial r}$ these potentials are directly correlated to the tip-substrate force which is in turn directly correlated to df , the signal obtained in the AFM measurements done in this thesis (an explanation of df is given in the next section). How $V(r)$, F and df are related to each other can be seen in figure 2.2.

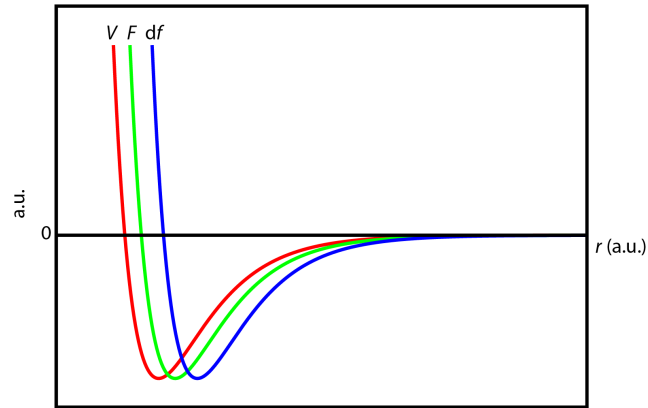


Figure 2.2: Plots of how the interaction energy (V), force (F) and the measured signal (Δf or df) are related to each other.

Though LJ and Morse potentials are often used in describing interparticle behaviour they are not exact. In the LJ potential only Pauli and vdW interactions are considered. These are not the only forces which play a role though. Electrostatic interactions, chemical bond formation and tip flexibility can also contribute to the observed tip-sample interaction. It is hard to quantify these interactions since the tip shape, termination and many more factors play a role. The general shape of the measured potentials is very similar to those described by LJ or Morse equations. Therefore, these other interactions have only recently been used in the description of AFM measurements [19].

Non contact AFM

The type of AFM technique used in this thesis is non contact AFM (nc-AFM). With this dynamic technique, the tip cantilever is actively vibrated at its eigenfrequency, f_0 . During the experiment the tip is brought in proximity to the substrate and raster scanned across the surface. Due to the tip-substrate interaction the eigenfrequency of the cantilever changes by a small amount, which is called df or Δf . In the experiments done in this thesis, a feedback system will try to keep the amplitude of oscillation constant, therefore this mode is called frequency modulated (FM) AFM. In this mode of operation, eq. 2.4, which relates df to the tip-substrate force, F , can be applied [26]:

$$\frac{df}{f_0} = -\frac{1}{\pi a k} \int_{-1}^1 F(z + a(1+u)) \frac{u}{\sqrt{1-u^2}} du \quad (2.4)$$

With k the spring constant of the cantilever, u the position of the tip, z the distance of closest approach between tip and sample and a the amplitude of oscillation. High resolution is achieved by using a small a and high f_0 . A high f_0 allows for more measuring points per second and a small a means that the signal measured is not an average over the whole LJ curve but only a small part of the curve. One way to control and measure f_0 is to make the tip cantilever of a piezoelectric material [27]. The properties of a tuning fork i.e. the high frequency stability and little energy consumption are also desired for the tip cantilever [24]. An example of a tip-sensor system which uses a quartz tuning fork is a qPlus sensor. Such a qPlus sensor consists of a needle which is mounted on one of the two prongs of the tuning fork. An example of a qPlus sensor can be seen in figure 2.3. With a qPlus sensor it is possible to simultaneously measure a tunneling current. In other words STM images can also be recorded with a qPlus sensor.



Figure 2.3: An example of a qPlus sensor. Note that one of the two prongs of the tuning fork is fixed to the white block. Image taken from ref. [24].

Just like in STM measurements there are two modes of operations: constant df AFM and constant height AFM. The first mode of operation is similar to constant current STM, a feedback loop tries to keep the df signal constant during scanning. The result is a topological map of the surface. The second mode of operation maps df at a constant tip-sample height. Unless otherwise stated all AFM images in this thesis are obtained using constant height mode.

2.1.3 Chemical identification

Not only an imaging technique, AFM can also be used to perform other types of experiments. One of these experiments is force-distance spectroscopy. As the name implies, the force is measured at different tip-sample heights. The obtained spectrum closely resembles the potentials plotted in figure 2.2. In these potentials the depth of well is unique for each combination of particles. So if spectra are taken above two different atoms in the substrate each should have a different minimum. In 2008 a difference in depth of well was found between Si, Sn and Pb atoms of a semiconductor material [20]. This technique was extended to differentiate between atoms in molecules [21]. It was proven one could measure a difference between a single N atom and neighbouring C atoms. During a measurement df is measured and not the force directly. Van der Heijden et al. find that you can also use these $df(z)$ spectra for chemical identification [21]. Therefore, those spectra will be used in this thesis as well.

2.2 Graphene

Graphene is a monolayer of sp^2 -hybridized carbon atoms which sit in a honeycomb crystal lattice. The crystal lattice can be described as two interpenetrating sublattices as can be seen in figure 2.4.

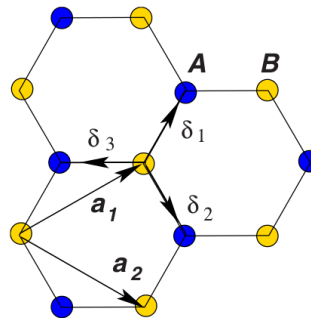


Figure 2.4: The crystal lattice of graphene. The two colours of the carbon atoms denote the two different sublattices which are usually called A and B. The lattice vectors are given by \mathbf{a}_1 and \mathbf{a}_2 . The nearest neighbour vectors are given by δ_1 , δ_2 and δ_3 . Image taken from ref. [7].

Because of the nature of sp^2 -carbon atoms and confinement in the z -dimension a 2-Dimensional Electron Gas (2DEG) is formed above and below the graphene. Combined with the honeycomb lattice this results in a very interesting band structure pictured in figure 2.5.

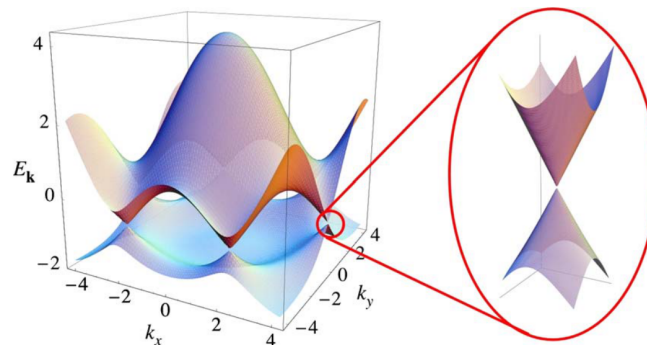


Figure 2.5: The band structure of graphene drawn in k -space. E_f is at the place the cones (sometimes named Dirac cones) touch, the K and K' points. Near the E_f the electrons behave like they have zero mass. Image taken from ref. [7].

Electrons near the E_f in graphene behave like they have zero mass and can be described by a linear dispersion relation [7]. Massless particles should go at relativistic speeds. Similar behavior is found in graphene where the electrons indeed move at these ballistic speeds [7].

One way to tune the electronic properties of graphene is by doping. Doping is the controlled addition of impurity atoms into the system which can alter the electronic properties of the material. In a similar fashion as in the regular semiconductor industry, one can think of n-type doping by addition of nitrogen atoms, or p-type doping by addition of boron atoms. However, how the dopant is bound to the graphene is crucial to the type of doping one will get. Knowledge of the structure of single dopants is therefore very important. In figure 2.6 examples are shown of the bonding of an N-dopant to graphene and the resulting doping type.

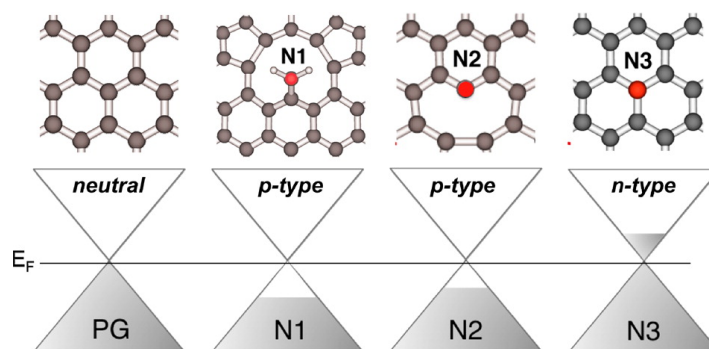


Figure 2.6: The different ways a N-dopant can be bound to graphene and the resulting doping type. PG stands for pristine graphene, N1 is also named nitrilic, N2 pyridinic and N3 graphitic doping. Image taken from ref. [11].

2.2.1 Synthesis of (doped) graphene

The first instance of isolated free standing graphene was made using regular scotch tape. [28] Using the scotch tape method, layer by layer of highly ordered pyrolytic graphite is peeled off until a monolayer (i.e. graphene) remains. Since this first isolation method, a lot of different techniques for the synthesis of (doped) graphene have been developed. Each technique belongs to one of two families: top-down or bottom-up. The studied graphene in this thesis was synthesized using a bottom-up approach.

In the bottom-up synthesis of graphene a precursor molecule (i.e. an organic molecule like ethylene) is dosed into an Ultra High Vacuum (UHV) system containing a substrate on which the graphene will be grown (for instance a Cu(111) or an Ir(111) crystal). The temperature of the substrate needs to be high enough to - in association with the possibly catalytic surface - break the bonds. After the heating the crystal is cooled. Although the exact synthesis mechanism is not fully understood, synthesis of large graphene flakes of over 200 nm have been reported [29]. Doping can be done post or during the synthesis of graphene. The post treatment usually involves bombarding pristine graphene with dopant ions and subsequent annealing [30]. Doping during synthesis can be achieved by altering the precursor (or precursors [31]). Instead of using a carbon based aromatic molecule a precursor containing the dopant atom is used. For instance pyridine can be used if one wants to make N-doped graphene [32]. One interesting effect that can happen during the bottom-up synthesis of doped graphene is the segregation of sublattice domains [32]. Segregation in this case means that the N-dopant will predominately site on one of the sublattice in each domain of graphene.

2.2.2 Graphene on a substrate

Due to the nature of the bottom-up synthesis the choice of substrate is very important. But also after synthesis the substrate plays a role in determining the properties of graphene.

Graphene and many of its substrates have a 3-fold symmetric lattice. Due to the lattice mismatch of graphene with the substrate the graphene layer is buckeled. This buckeling of graphene is periodic and the resulting pattern is called the Moiré pattern. The height difference between the top sites and the valley sites in the Moiré pattern is approximately 30 pm [33]. Just like in a regular crystal lattice, the Moiré lattice also has a unit cell. An example of this cell can be seen in appendix A1 where the high symmetry positions of the Moiré cell are shown.

This buckeling can affect the electronic properties of the graphene. For instance, it is known that graphene on an Ir(111) crystal has a periodic electronic modulation with the surface [33]. The top sites of the Moiré pattern are weakly interacting with the surface and the valley sites are more strongly bound to the surface. This modulation in the substrate-graphene interaction can be seen in figure 2.7.

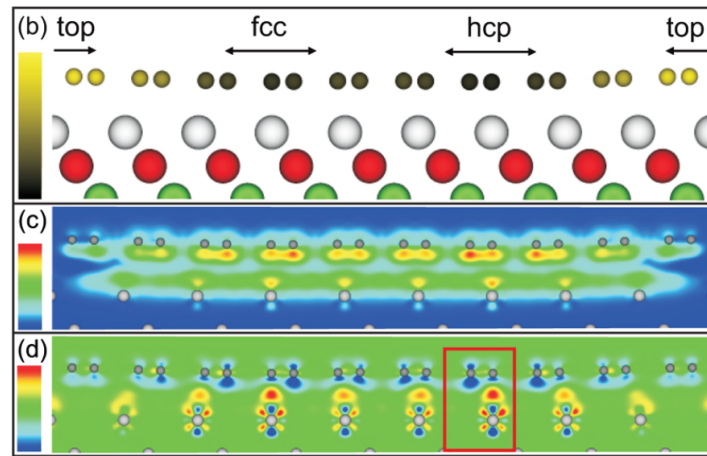


Figure 2.7: The modulation of the electronic structure of graphene. An increase in electronic density (i.e. associated with a chemical bond) can be seen in the regions where the graphene is close to the surface (inside red square). Image taken from ref. [33].

DFT calculations show that the increase in electronic density between substrate and graphene is still there if we have N-doped graphene [22].

Chapter 3

Experimental section

In this chapter the experimental methods used in this thesis are described. The first part discusses the synthesis of doped graphene. For this synthesis a custom built setup was used. Besides the details of this setup, also the reaction conditions will be described. The second part discusses the characterization methods of the as-synthesized graphene. Here, the scanning probe measurements will be explained and how chemical identification was achieved.

3.1 Graphene synthesis

N-doped graphene was made using a bottom-up synthesis technique. For this purpose a custom built experimental setup was used. The whole synthesis setup was kept at Ultra High Vacuum (UHV) conditions with typical base pressures of $1.0 \cdot 10^{-10}$ mbar. The setup was structured in the following way: two manipulator arms were connected to a vacuum chamber. In one arm a cup with the precursors was held whilst in the other arm the crystal was stored. The crystal was placed above a filament in its arm. This arrangement allows for heating of the crystal to 1200 °C. Another advantage is that the arm containing the precursor can be put into and out of the vacuum chamber at any moment. This allows for preheating of the crystal without fear of premature evaporation of molecules. An image of the setup with the synthesis in action can be seen in figure 3.1 .

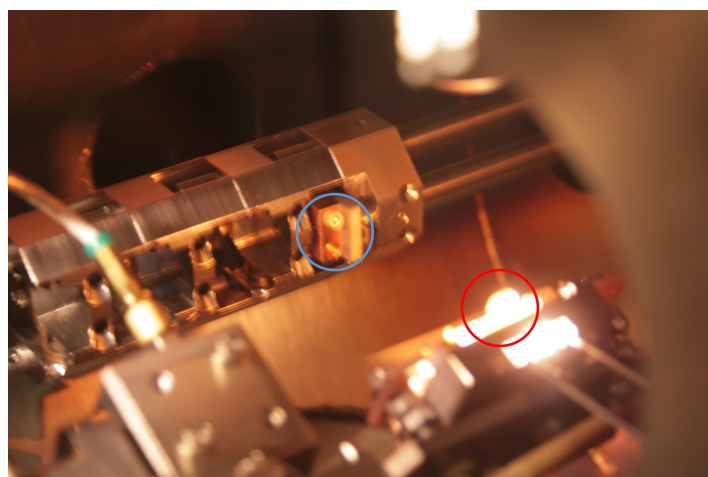


Figure 3.1: Photo of the synthesis setup. In the blue circle the cup holding the precursor molecules can be seen. In the red circle is the sample plate with the heated crystal facing the cup.

The crystals used as substrates were atomically flat Cu(111) and Ir(111) crystals. These surfaces were cleaned by repeated cycles of sputtering (with Ar^+ ions) and annealing. Two types of precursor molecules were used. In figures 3.2a and 3.2b the chemical structures of 1,10-phenanthroline (Phen) and 1,2,4-Triazolo[1,5-a]pyrimidine (Pyr) respectively are shown. The precursors were purchased from Sigma-Aldrich and had a purity of $\geq 99\%$ for Phen and 99 % for Pyr. Both these precursors are solids under

UHV conditions. This allows for storage in the precursor arm and easy handling in the current synthesis setup.

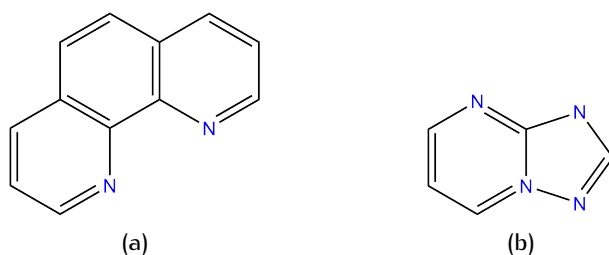


Figure 3.2: (a) 1,10-phenanthroline (Phen) (b) 1,2,4-Triazolo[1,5-a]pyrimidine (Pyr)

For the synthesis of N-doped graphene on Cu(111) a protocol from Zabet-Khosousi et al. was adapted [32]. This synthesis should yield graphitic N-dopants (figure 2.6). The crystal was preheated to 875 °C approximately for 10 min. After preheating, the precursor arm was brought into the vacuum chamber and put in front of the crystal. Due to the heat of the filament and crystal the molecules (only Phen was used in the synthesis on Cu(111)) started to evaporate almost immediately. This could be monitored by the increase in pressure from $4.9 \cdot 10^{-8}$ mbar at the start to $9.9 \cdot 10^{-8}$ mbar after 90 s. After 90 s the evaporation was stopped by retraction of the precursor arm. The crystal was annealed at 875 °C for 20 min.

N-doped graphene on Ir(111) was synthesized with the same setup as described above. However, the reaction conditions were slightly different with respect to synthesis on Cu(111). As the synthesis on Ir(111) was based on the synthesis of pristine graphene on Ir(111) using ethylene gas as described by ref. [34]. The main difference was that the Ir(111) was not preheated like the Cu(111) crystal was. Instead, the temperature of the crystal was raised to 1200 °C and the precursor arm was immediately put in front of the Ir(111) crystal. After evaporation the precursor arm was retracted and the crystal was annealed for 30 s. The Ir crystal was transferred out of the vacuum chamber at elevated temperatures to minimize the adsorption of residual molecules to the surface. For this synthesis both precursors were used (not together at the same time). For convenient comparison all synthesis can be seen in table 3.1.

Table 3.1: Variations in reaction conditions

Substrate	Precursor	Evaporation time (s)	Pressure after evaporation (mbar)	Annealing time
Cu	Phen	90	$9.9 \cdot 10^{-8}$	20 min
Ir	Phen	25	$5.3 \cdot 10^{-8}$	30 s
Ir	Pyr	10	$5 \cdot 10^{-8}$	30 s

3.2 Scanning Probe Measurements

SPM measurements were performed on an Omicron Low Temperature (LT) Microscope operating at cryogenic temperatures (4.5 K) in UHV conditions. A photo of the outside of the LT microscope can be seen in figure 3.3.

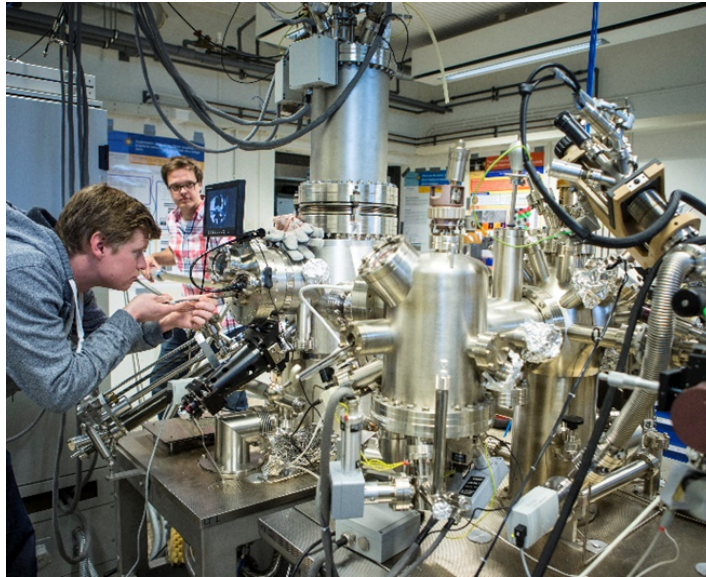


Figure 3.3: Image of the complex arrangement of vacuum chambers which contain the scanning probe microscope.

The big 'tower' in the top centre of the photo is the cryostat containing liquid He and liquid N used for cooling. Slightly underneath the cryostat is the measuring part of the microscope. This part contains the scanner, sensor and sample. Which are thermally connected to the cryostat by copper braids. This whole experimental setup is placed on a table which is in turn placed on an active vibration compensation system. This system actively suppresses vibrations from the surroundings. The suppression with this system is combined with the internal suspension of the stage, using long springs. This combination allows for a resolution in z of 3 pm at cryogenic temperatures.

Atomically sharp tips were prepared by repeated crashing and melting with the clean crystal surfaces. In this fashion the W tip is coated with a Cu or Ir layer depending on which sample is in the microscope. The STM measurements were performed using a reverse bias setup. This means the applied voltage across the tunneling junction is applied with respect to the tip (the tip is ground). The tunneling current is low pass filtered before it is recorded. The parameters that were altered during the measurements were the gap voltage and the tunneling current setpoint (I_{set}). All the STM measurements were done in constant current unless stated otherwise. SPM measurements were performed using a qPlus sensor. A Phase Lock Loop (PLL) kept the amplitude constant (FM AFM) by applying a modulation frequency (df). This modulation frequency is proportional to the tip-substrate force (eq 2.4). For each AFM measurement the tip had an eigenfrequency, $f_0 \approx 25\text{kHz}$, a spring constant, $k \approx 1800\text{ N/m}$ and a quality factor, $Q \approx 25\text{ kHz}$. All AFM measurements in this thesis are done in constant height mode.

Image processing

All the obtained scanning probe images were analyzed in the following way: the image is averaged over the trace and the retrace, then a polynomial plane is subtracted (this procedure was not done for

AFM images). Finally a convolution filter is applied using a kernel of the form: $\frac{1}{9} \begin{pmatrix} 1 & 1 & 1 \\ 1 & 1 & 1 \\ 1 & 1 & 1 \end{pmatrix}$.

3.2.1 Chemical identification

Chemical identification measurements were performed by taking single $df(z)$ -spectra of (possible) nitrogen atoms and carbon atoms. Any differences between these spectra would indicate the possibility for chemical identification. For fair comparison between the N and C spectra, the C spectra are usually taken on C atoms which have a similar place in the Moiré cell as the probed N candidate.

Constant Height Stacks

Complementary to the single $df(z)$ spectra is a Constant Height Stack (CHS). A CHS can be considered a form of grid spectroscopy. With grid spectroscopy, spectra are taken on a pre-set grid over the surface. With grid spectroscopy the spectra are obtained immediately for each pixel while with a CHS the spectra are obtained via post measurement data processing from the data cube. An AFM image in constant height is measured very close to the substrate. After this image the tip is raised by a small height step (Δz) and another AFM image is taken. By doing this many times a stack of AFM images is obtained. Every column in this cube of data represents a $df(z)$ -spectrum. These CHS measurements were performed in an automated manner. For this purpose a script in the Python programming language was written (Python2.7).

This CHS script worked in the following manner. At scan one an STM image is taken which will be used for the semi-active drift compensation. We call it semi-active drift compensation since only in between scans is drift compensation applied. After the first STM scan, the feedback signal is turned off and the tip is lowered to a z_{start} height and the first AFM scan is taken. After this AFM scan the feedback system is turned on again an another STM image is taken. From both the first and the second STM images polynomial planes are subtracted using the flatten function of the SPIEPy package. The first and second STM scans are compared using the correlate2D function of the SciPy package to see if there is any drift. If there is, the scan window is moved to compensate. This loop of AFM and STM scans repeats itself during the full CHS. Note that every STM image is compared to the first STM image. This script made use of different Python packages. Besides the before mentioned packages also the access2theMatrix package was used. This package allows for the control of the Matrix software which controls the LT microscope.

Heightstacks were analyzed in the following fashion: in every spectrum of the stack the minimum value of the well was found. From this minimum 5 points in $-z$ and $+z$ were used for fitting with a parabolic function. For this fitting the polyfit function of the NumPy package was used. From these polynomial fits the position of the minimum was determined (both in df and z). These values were put into two maps: a df -map and a z -map. The df -map contains the depth of the well at each pixel. This map should point to the location of a N atom. Also knowledge on the extent the N atom has on graphene is in this map. The z -map contains the position of the well on the z -axis of each pixel. This map should follow the Moiré pattern and might show to what extent the N-dopants distort this pattern.

3.2.2 The strategy

N atoms have a characteristic signature in STM images [23]. This signature is exploited in the measurements. First a N atom is found in STM mode. After this, the process of chemical identification, as described above, is applied. Since we should have the clear signature of the STM image we have a built in control experiment.

Chapter 4

Results and discussion

This chapter discusses the obtained results. The first part describes the results of the experiments on N-doped graphene on Cu(111). The second part discusses the results of the experiments on N-doped graphene on Ir(111) where some peculiarities were found. Furthermore, we try to explain similarities and differences between the DFT calculations (appendix C1) and both sets of experiments.

4.1 N-doped graphene on Cu(111)

The graphene on Cu(111) sample consisted of many small patches of graphene. A typical STM image of N-doped graphene on Cu(111) is shown in figure 4.1.

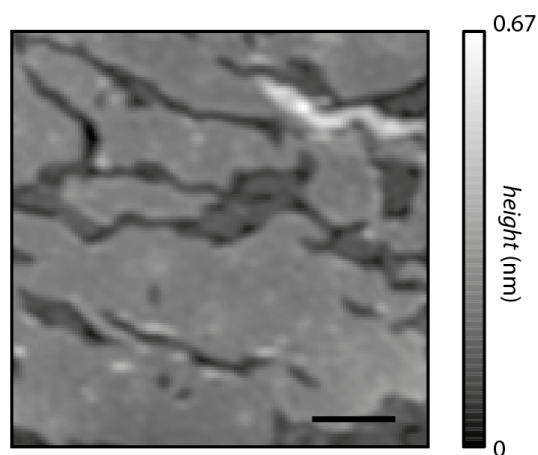


Figure 4.1: STM image of N-doped graphene on Cu(111) (obtained at 100 mV and 20 pA). Scalebar corresponds to 10 nm.

The graphene on Cu(111) showed many grain boundaries between the multiple graphene domains. Why this is observed and not the big patches of graphene of hundreds of nanometers reported by Zabet-Khosousi et al. is unknown [32]. Further investigation falls outside the scope of this thesis, so these questions were not further pursued. An STM image and the corresponding AFM image on a small piece of N-doped graphene can be seen in figure 4.2.

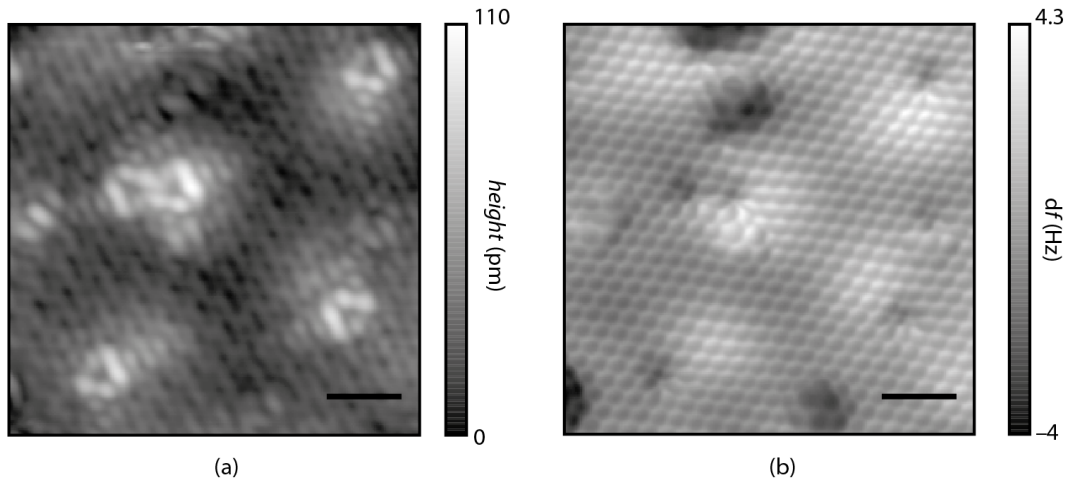


Figure 4.2: (a) STM image of N-doped graphene on Cu(111) (obtained at 1.00 V and 50 pA). (b) AFM image ($z_{offset} = -130$ pm w.r.t. to an STM setpoint at 50 pA and 1 V) of exactly the same area as the STM image of a. Scalebars correspond to 1 nm.

The observed hollow triangular features in the STM image of figure 4.2a correspond very well in size and shape from previous experiments on N-doped graphene [23, 30, 32]. The two observed orientations of the triangles are usually attributed to the two possible dopant positions of the dopant atom (sublattice A or B) [32]. In figure 4.2b an AFM image of the same area as the STM image of figure 4.2a can be seen. On every place there is a N atom according to the STM image, the AFM image is perceived distorted. From DFT calculations it is known that the C-N bond lengths are almost exactly the same as the C-C bond lengths in graphene [22]. For this reason it is likely that these distortions are not truly present in the lattice. Instead, these distortions could be due to a tip effect. Furthermore, if we closely look at the graphene lattice in figure 4.2b we still find 3-fold symmetry around each distortion. This would point towards graphitic doping (N3 in figure 2.6). Also the fact we don't see any reorganisations in the lattice surrounding the N atom points in this direction. Though the STM image clearly shows triangular features which are similar to those which have been found before, the contrast of the rest of the lattice is quite peculiar: neither the rings nor the benzene rings can be clearly distinguished. Similarly, in the AFM image the honeycomb lattice can be seen in great detail but this contrast is uncommon. Therefore, we cannot say with certainty what tip termination we have. Nevertheless, the observed resolution is high. On single N-dopants $df(z)$ -spectra were taken, figure 4.3.

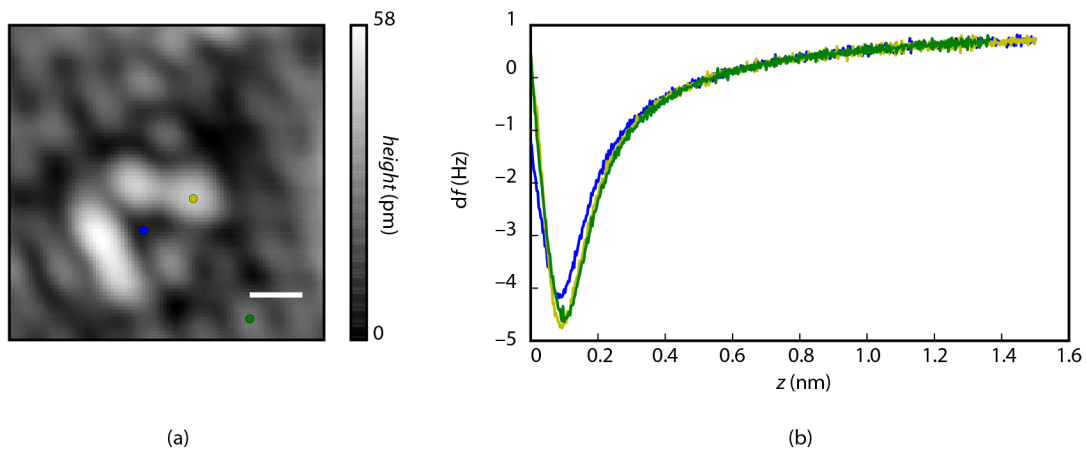


Figure 4.3: (a) STM image of the local area of a single N-dopant (obtained at 10 pA and 1.00 V) The coloured dots indicate positions at which $df(z)$ -spectra are taken. The scalebar corresponds to 2.5 Å. (b) $df(z)$ -spectra at positions indicated in (a). The colour corresponds to the coloured dot which marks the location in the STM image.

The blue spectrum, which corresponds to the N atom, is clearly different from the spectra on the neighbouring C atoms. It is quite peculiar that the depth of the N-well is less negative than of the spectra obtained over the C atoms. Van der Heijden et al. find an reverse trend for a N atom in a organic molecule [21]. The depth of the spectrum taken over the N atom is in their case lower for the N atom than for the neighbouring C atoms. For the cause of this trend we have to have a more in depth knowledge on the contrast formation mechanism at work. For now we can only speculate on the reason. A possible reason could be a different charge distribution around the N-dopant. A different interaction of the organic layer with the metallic substrate for graphene compared to the molecule is another option. Or a different tip termination might be the cause (in their experiment a well defined CO tip is used whilst here we don't know the tip termination). A lot of questions are still open, though a difference between the spectra has been shown.

4.1.1 Mapping a single dopant

In figure 4.4 the results of a CHS of a N-dopant in graphene on Cu(111) are shown. In the df -map of figure 4.4b a clear contrast can be observed at the place where the N atom is. From the STM image of figure 4.4a it can be seen that the N atom affects the electronic states multiple lattice sites away. We find a similar delocalization in the df -map where the direct neighbours of the nitrogen have a different well depth than other lattice C atoms which do not seem to be affected by the N-dopant. In both the z -map, figure 4.4c and the df -map the Moiré pattern can be clearly identified. The fact that the Moiré pattern can be seen in the df -map is of interest since this further indicates the different chemical identity of the atoms in the Moiré unit cell. This different chemical identity is due to the different van der Waals (vdW) background the different atomic positions have in the Moiré pattern. Despite this effect where the C atoms are all slightly different, chemical identification is still possible since the N atom still appears clear in the df -map. To exclude the different vdW background of the different atoms in the Moiré cell spectra from the CHS are extracted over atoms in similar positions. In figure 4.4d the locations of these spectra are indicated. The blue star corresponds to the N atom and the yellow markers correspond to C atoms on similar positions in the Moiré cell (similar graphene-substrate heights).

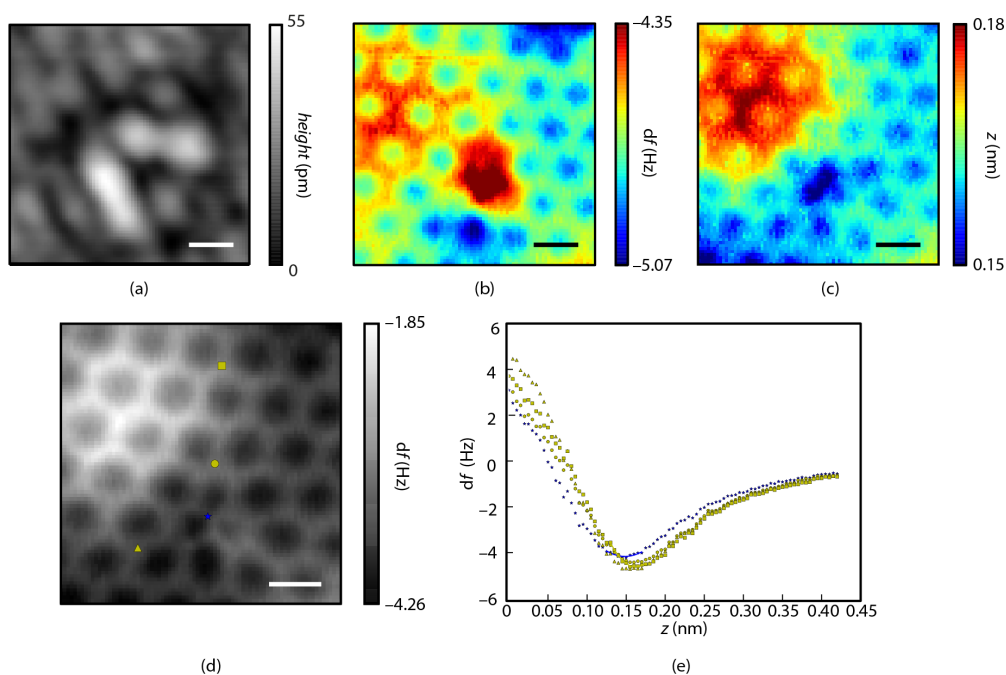


Figure 4.4: (a) STM image of the N-dopant. (b) df -map. A map of the well depth on every pixel. (c) z -map. A map of the z -axis position of the well. (d) A constant height AFM image taken from the stack. The markers indicated positions on which individual spectra are taken. (a-d) Scalebars corresponds to 2.5 Å. (e) The spectra belonging to the positions of the markers. The solid lines are the parabolic fits.

The spectra in figure 4.4d are very similar in well depth to the spectra of figure 4.3b. Also a difference in the z -positions of the wells can be distinguished clearly from these spectra. This indicates that besides the depth of the well also the z -axis position can be used for chemical identification.

In appendix B1 a CHS on a different N-dopant (different sublattice) are shown. Tip termination in appendix B1 was the same as the tip termination in figures 4.3 and 4.4. The results are very similar to each other. This result is unsurprising since both sublattices are equivalent and so should in principle yield the same results.

4.2 N-doped graphene on Ir(111)

Typical examples of the different graphene on Ir(111) samples can be seen in figure 4.5. These two types of samples were prepared with two different precursors, 1,10-phenanthroline (Phen) and 1,2,4-Triazolo[1,5-*a*]pyrimidine (Pyr). Phen is the same precursor used in the synthesis of N-doped graphene on Cu(111). The graphene sample of figure 4.5a was prepared using Pyr as precursor and of figure 4.5b using Phen as precursor respectively.

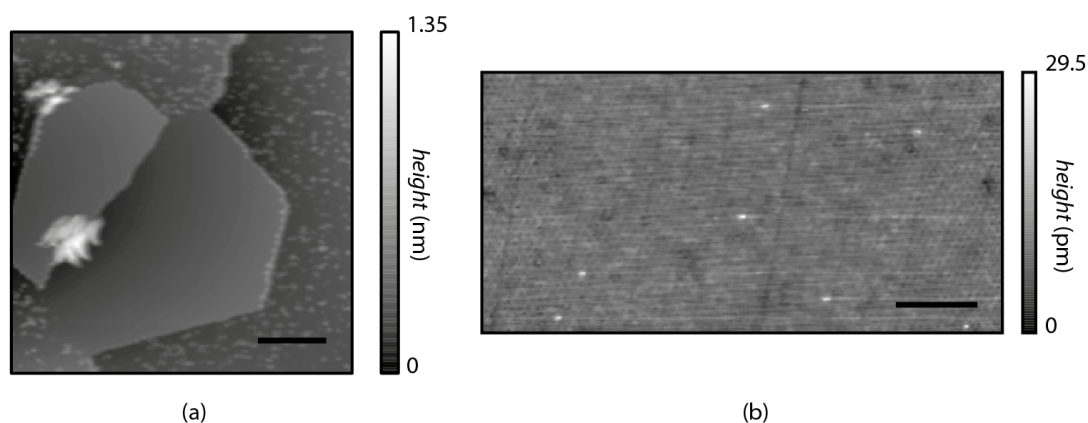


Figure 4.5: (a) STM image of a graphene flake found on the sample prepared using Pyr as precursor. (b) STM image of a patch of graphene found on the sample prepared using Phen as precursor. (a,b) Scalebars correspond to 25 nm. Images obtained at 100 mV and 1 nA.

The graphene samples were rather different. The sample of figure 4.5a contains mostly these well defined graphene flakes with a diameter of about 100 nm which are rather homogenously distributed across the surface. In figure 4.5b the graphene patches were several hundreds of nm in size with many areas of hundreds of nm up to a micrometer in size of clean Ir crystal in between the patches of graphene. In literature these kinds of structures are also found [34]. They attribute the differences to different annealing times. In the cases presented here both samples were annealed for 30 s. Therefore, it is rather notable that these well defined classes are observed. The doping grade seems to be much lower for the graphene on Ir(111) samples than for the graphene on Cu(111) sample. A possible explanation for this is that due to the higher temperature in the synthesis of graphene on Ir(111) w.r.t. the synthesis of graphene on Cu(111) the reaction intermediates are much more mobile. It is likely that two very mobile N atoms react faster to the very stable N_2 than two less mobile ones. Why we have these two different types of samples is an interesting question but falls outside the scope of this thesis. The most important conclusion is that N-doped graphene on Ir(111) has been successfully synthesized in both samples.

4.2.1 Chemically identifying single dopants

The graphene investigated here is the sample of figure 4.5b. In figure 4.6 the results of a CHS on two features can be seen. In the STM image of figure 4.6a the two features show similarities to the features found on the N-doped graphene on Cu(111). The positions where the triangles are seen in the STM image also show clearly in the df -map of figure 4.6b. The positions of the triangles near the top sites of the Moiré cell makes analysis of these results non trivial; since their positions near these top sites makes the top sites look elongated and not perfectly spherical. Elongation of features in regular SPM images can be caused by thermal drift. Since not every top site has the same elongation and combined with the fact that the contrast coincides with the triangles of the STM image, makes the drift as a major component to the observed shapes a less reasonable explanation. Though we cannot exclude drift effects entirely.

The found less negative values for the depth of the wells of the possible N atoms is similar to that which is observed for the graphene on Cu(111) experiments. Although the N atoms found here are not exactly on a top site or valley site we can still qualitatively compare them with the performed DFT calculations (appendix C). The trends found in these calculations (the N atom has a higher depth of well than the C atom) is also found here. We are not sure what sort of tip termination we have and therefore we cannot say anything with certainty on the contrast formation mechanism at work here. The DFT calculations show that an increase in electron density is observed between the tip and the probed atom [22]. Since we see the same trend in df here as in the DFT calculations this chemical bond formation might also happen here. Since the N atoms are not exactly in a valley site (HCP or FCC site appendix A) we cannot see an effect of the chemical bond between the valley site atoms and the substrate. And therefore we cannot say anything on the effects on chemical identification of the chemical bond between the substrate and graphene.

Chemical identification also works on N-doped graphene on Ir(111) and the results are similar to what we see on N-doped graphene on Ir(111).

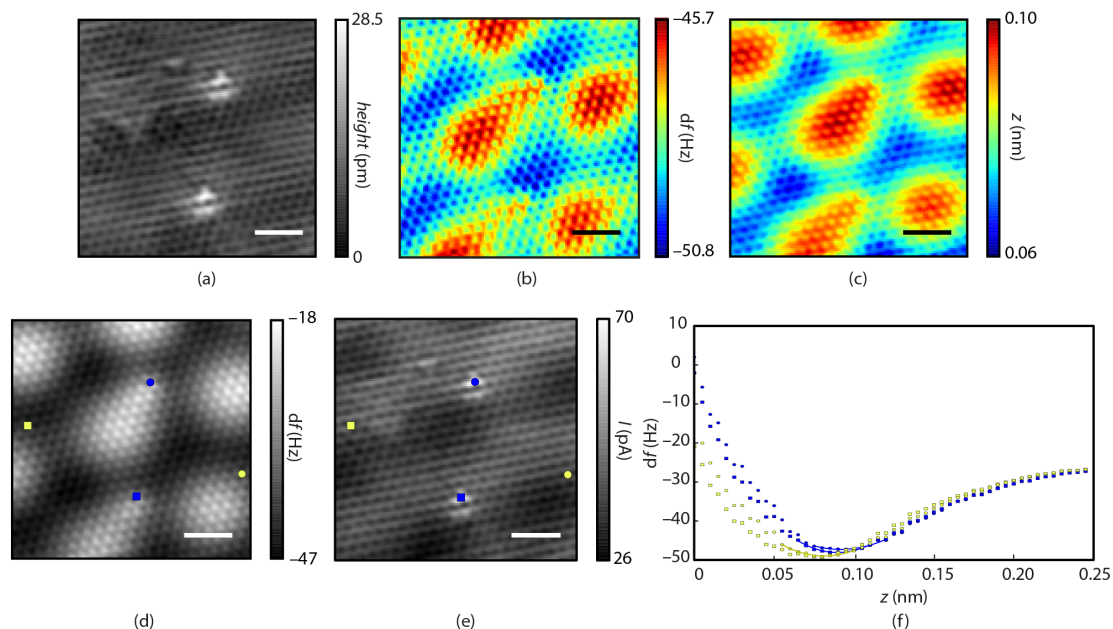


Figure 4.6: (a) STM image of two possible N atoms (100 mV and 1 nA). (b) df -map. A map of the well depth on every pixel. (c) z -map. A map of the z -axis position of the well. (d) AFM image and (e) corresponding I -image taken from the CHS. The markers indicated positions on which individual spectra are taken. (a-e) Scalebars correspond to 1 nm. (f) The spectra belonging to the positions of the markers. The solid lines are the parabolic fits.

4.2.2 Double dopants?

The graphene samples in this section were synthesized using Pyr as precursor. An example of a feature found in the graphene on Ir(111) sample is shown in figure 4.7.

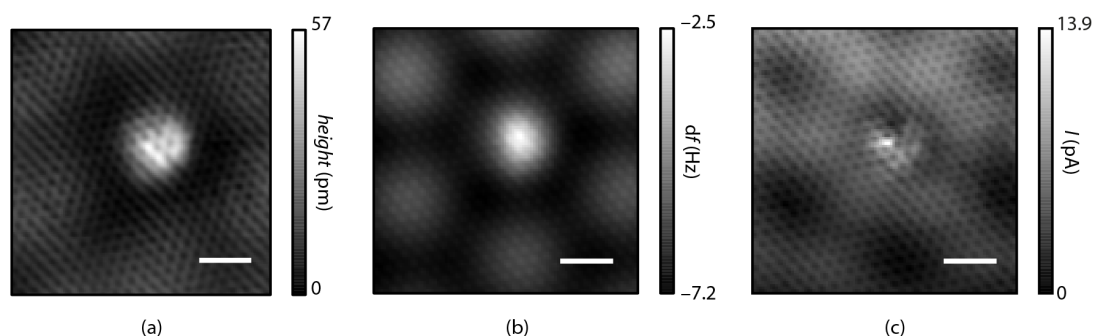


Figure 4.7: (a) STM image of a possible N-dopant in graphene (100 mV and 1 nA). (b) Constant height AFM image of the same location. (c) Constant height STM image recorded during the AFM measurement. (a-c) Scalebars correspond to 1 nm.

The shape of the feature in the STM image of figure 4.7a looks like a distorted triangle. One possible explanation for this comes from Telychko et al. [30]. They have observed somewhat similar features in N-doped graphene on SiC. They ascribe these features to two N-dopants sitting one C away from each other. The size of this feature (approximately 1 nm) is larger than those found in N-doped graphene on Cu(111) and it's also larger than the features in figure 4.6a (both these features have approximately the size of 0.5 nm). The used precursor (Pyr) for this sample possesses this structure of two N atoms sitting one C atom away from each other. It would be interesting to see if we indeed have such a structure present as this might give insights into the reaction mechanism. In the AFM image of 4.7b the feature appears very bright which is rather interesting since this is not found in N-doped graphene on Cu(111). It could be that due to two N atoms next to each other the lattice protrudes upwards with little distortion in the lateral dimensions. Unlike the AFM image on the Cu(111) substrate, the lattice around this feature in the AFM image of figure 4.2b does not seem to be distorted. This suggests that the tip termination is different in these experiments compared to the tip termination for the experiments on the Cu(111) surface. Another striking difference in this AFM image compared to the results on Cu(111) is that the lattice isn't visible. Instead the benzene rings are imaged. It is known that this is tip dependent [35]. In the constant height STM image of figure 4.7c the feature appears less bright than in the constant current STM image of figure 4.7a. In the I -image of figure 4.7c a 'V shape' can be distinguished. This would suggest that the intersection of the V is the bridging C atom with the two N atoms making up the lines of the V shape. To get more information on this feature a CHS was taken. The results are shown in figure 4.8.

In both the df - and z -maps of figures 4.8a and 4.8b the feature also observed in the STM image appears very clear. The full top site appears a lot brighter at the place where the possible N atoms are, compared to the other top sites. The bright red spot observed in figure 4.8b is similar in size to the feature observed in figure 4.8a. In the spectra of the CHS in figure 4.8f a clear difference can be seen in the minima of the wells. The contrast observed in the df -map of figure 4.8b extends across four rings of which one ring appears somewhat less bright. If just three rings appeared bright than this would point to a single dopant. But since there is a fourth ring which also adds to the contrast, the possibility of two dopants next to each other cannot be excluded.

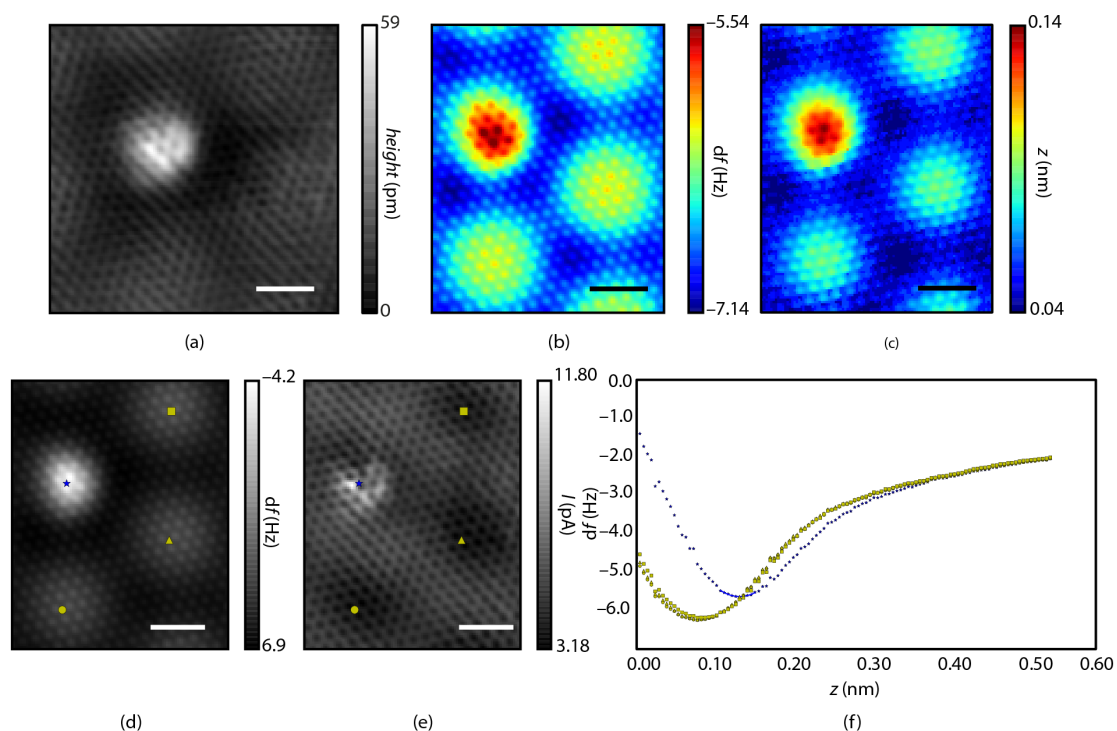


Figure 4.8: (a) STM image of the probed N atom. (b) df -map (c) z -map (d) An AFM image taken from the stack. The markers indicated positions on which individual spectra are taken. (e) Constant height I -image taken from the CHS. The height is the same as the constant height AFM image of (d). (a-e) Scalebars correspond to 1 nm. (f) The spectra belonging to the positions of the markers. The solid lines are the parabolic fits.

In the same sample and with a different tip termination as figure 4.8 another feature is found which is shown in figure 4.9. The STM images of both figures are somewhat different (figures 4.8a and 4.9a). The most striking difference is that this feature appears way less bright than the one described above. Though this striking difference is observed, there are also some similarities. These similarities are especially striking if we compare the constant height I -image of figure 4.8e with the STM image of figure 4.9a. The AFM image from the CHS of figure 4.9d is very similar to the AFM image of 4.7a suggesting that both features are the same. Though it is interesting that we cannot see the feature in the I -image of figure 4.9e as clear as in the I -image of figure 4.8e. The spectra taken from the CHS of figure 4.9f are also very similar to the spectra from figure 4.8f.

These similarities would suggest that both features are caused by the same doping structure. And that the observed contrast differences in both STM images are due to different tip terminations. In the df -map of figure 4.9b we can very clearly see the Moiré pattern. The resolution is so high, we can even distinguish between FCC and HCP valley sites (the HCP sites have lower df values than the FCC sites). In the middle top site the feature appears very brightly. These top site atoms have higher df values than the atoms on different top sites. The contrast isn't homogenously distributed as you would expect if you have a single N dopant. Instead the contrast around the feature looks somewhat elongated. This would also point to the possibility of two dopants sitting next to each other.

Since the N atoms are on a top site in this measurement we cannot see the effect of chemical binding of graphene with Ir. As with the measurements of figure 4.8, the lattice isn't visible but the benzene rings are. As mentioned before, this effect of imaging rings or lattice has been found before and is very dependant on tip termination. The fact we see a higher df value for the N atoms here as well supports the universality of chemical identification. With different tip terminations we get similar results which are in good agreement with DFT calculations.

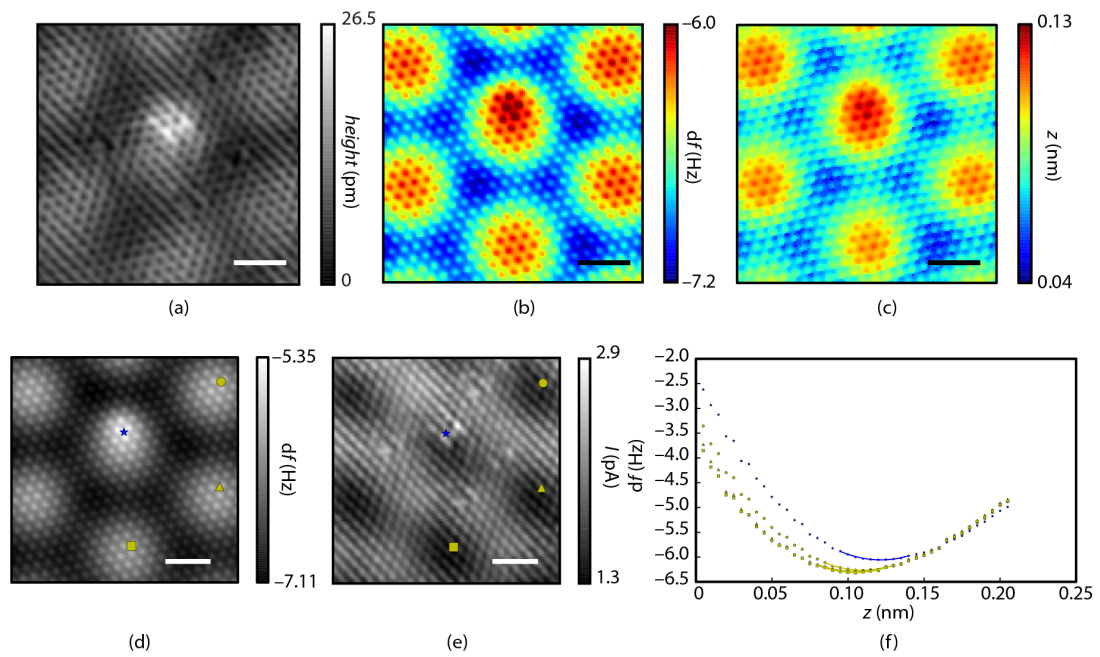


Figure 4.9: (a) STM image of the probed N atom. (b) df -map (c) z -map (d) An AFM image taken from the stack. The markers indicated positions on which individual spectra are taken. (e) Constant height I -image taken from the CHS. The height is the same as the constant height AFM image of (d). (a-e) Scalebars correspond to 1 nm. (f) The spectra belonging to the positions of the markers. The solid lines are the parabolic fits.

Chapter 5

Conclusions and outlook

Chemical identification was successfully achieved by AFM in the study of N-dopants in graphene. Independent of tip termination or substrate the $df(z)$ -spectra gave similar results. The observed trend in the $df(z)$ -spectra is the same throughout, dominant over these other effects. This is also in agreement with DFT calculations. How the obtained results relate to the properties of a single dopant is not yet known.

To answer this, it could be useful to combine experiment with more extensive computational modelling. For instance Jelinek et al. have developed a model which can be used to simulate AFM images [36]. This model can take a variety of different effects into account like tip charge, tip flexibility etc. Such a model might give insights into important factors, such as the charge distribution around the N-dopant.

Also experimental techniques can be used to gain insight on this topic. One of these techniques is Kelvin Probe Force Microscopy (KPFM). Recently KPFM has been used to map the charge distribution in a molecular system [18]. It would be interesting to see if, with the same tip, KPFM and CHS measurements can be applied to the same dopant and see how they compare. This will give insight if charge distribution is important in the contrast formation mechanism.

The place of the dopant in the Moiré cell seems to be of little effect to the results of chemical identification. But to be sure of this, more research is required. Single spectra or CHS measurements on a N-dopant on more or less exactly a valley site and a top site have to be done and see how they compare to measurements on pure C sites to answer this question. This should also give more knowledge as to how the chemical bond between a valley site atom and the Ir(111) substrate affects chemical identification.

By changing the tip to a well defined tip like CO or Xe we can see how the tip plays a role in chemical identification. For these tips we know important properties like tip charge, vdW's radius etc. So using these tips will tell us something on the importance of these variables and how they affect the observed contrast.

Another alteration one could expand into is the changing of the dopant atom. For this B-doped graphene is an interesting candidate. Since the B atom has two electrons less than a N atom it is expected to have a significant influence on the process of chemical identification. An effect that could happen is the changing of the contrast on the dopant from a higher value for df in the well w.r.t to the C atoms to a lower value for df in the well.

Although more research is required to answer some of these questions. The answers to these questions will, without a doubt, lead to a deeper understanding of chemical identification and with that to the properties of dopants in graphene. Therefore, chemical identification can already be considered as a tool for the study of doped graphene.

Acknowledgements

There are many people who have contributed in a small or big way to this thesis. All of these people deserve a big THANK YOU.

The first person is *Nadine*. Without your supervision I wouldn't have anything to write about. The second person is *Ingmar*. Thanks for being so kind enough to have me in the Basement crew. Then there is *Joost*. A big thanks for helping me with Python and putting me in my place by calling me *student*. Every chemist needs a smart physicist. My smart physicist is *Gaeatano* who did all the theoretical work. Lastly I would like to thank the whole CMI group for making my time enjoyable and for putting up with my stupid jokes.

Bibliography

- [1] M. Faraday, *Philosophical Transactions of the Royal Society of London*, 1857, **147**, 145–181.
- [2] T. Razykov, C. Ferekides, D. Morel, E. Stefanakos, H. Ullal and H. Upadhyaya, *Solar Energy*, 2011, **85**, 1580–1608.
- [3] E. de Smit, I. Swart, J. F. Creemer, G. Hovelings, M. Gilles, T. Tylliszczak, P. Kooyman, H. Zandbergen, C. Morin, B. Weckhuysen and F. de Groot, *Nature*, 2008, **456**, 222–225.
- [4] C. Berger, Z. Song, T. Li, X. Li, A. Y. Ogbazghi, R. Feng, Z. Dai, A. N. Marchenkov, E. H. Conrad, P. N. First and W. a. de Heer, *The Journal of Physical Chemistry B*, 2004, **108**, 19912–19916.
- [5] M. C. Daniel and D. Astruc, *Chemical Reviews*, 2004, **104**, 293–346.
- [6] R. Feynman, *There is plenty of room at the bottom*, 1959.
- [7] a. H. Castro Neto, N. M. R. Peres, K. S. Novoselov and a. K. Geim, *Reviews of Modern Physics*, 2009, **81**, 109–162.
- [8] X. Li, X. Wang, L. Zhang, S. Lee, H. Dai, L. Zhang, S. Lee and H. Daif, *Science*, 2008, **319**, 1229–1232.
- [9] P. Vogt, P. De Padova, C. Quaresima, J. Avila, E. Frantzeskakis, M. C. Asensio, A. Resta, B. Ealet and G. Le Lay, *Physical Review Letters*, 2012, **108**, 155501.
- [10] H. Liu, A. T. Neal, Z. Zhu, Z. Luo, X. Xu, D. Tomanek and P. D. Ye, *ACS nano*, 2014, **8**, 4033–4041.
- [11] T. Schiros, D. Nordlund, L. Pa, D. Prezzi, L. Zhao, K. S. Kim, U. Wurstbauer, C. Gutie, D. DeLongchamp, C. Jaye, D. Fischer, H. Ogasawara, L. G. M. Pettersson, D. R. Reichman, P. Kim, M. S. Hybertsen and A. N. Pasupathy, *Nano letters*, 2012, 4025–4031.
- [12] M. J. Rust, M. Bates and X. Zhuang, *Nature Methods*, 2006, **3**, 793–796.
- [13] S. Stankovich, D. a. Dikin, R. D. Piner, K. a. Kohlhaas, A. Kleinhammes, Y. Jia, Y. Wu, S. T. Nguyen and R. S. Ruoff, *Carbon*, 2007, **45**, 1558–1565.
- [14] G. Binnig, H. Rohrer, C. Gerber and E. Weibel, *Physical review letters*, 1982, **49**, 57–61.
- [15] G. Binnig and C. F. Quate, *Physical Review Letters*, 1986, **56**, 930–933.
- [16] G. Binnig, H. Rohrer, C. Gerber and E. Weibel, *Physical Review Letters*, 1983, **50**, 120–123.
- [17] L. Gross, F. Mohn, N. Moll, P. Liljeroth and G. Meyer, *Science*, 2009, **325**, 1110–1114.
- [18] F. Mohn, L. Gross, N. Moll and G. Meyer, *Nature Nanotechnology*, 2012, **7**, 227–231.
- [19] S. K. Hämäläinen, N. van der Heijden, J. van der Lit, S. den Hartog, P. Liljeroth and I. Swart, *Physical Review Letters*, 2014, **113**, 186102.
- [20] Y. Sugimoto, P. Pou, M. Abe, P. Jelinek, R. Pérez, S. Morita and O. Custance, *Nature*, 2007, **446**, 64–7.
- [21] N. Van der Heijden, P. Hapala, J. Rombouts, J. van der Lit, D. Smith, P. Mutombo, M. Švec, P. Jelinek and I. Swart, *Submitted*, 2016.

- [22] Calogero, G, *A van der Waals Density Functional study of N-doped graphene/Ir(111) For Chemical Identification of individual atoms with AFM and STM*, Utrecht University, 2015.
- [23] L. Zhao, R. He, K. T. Rim, T. Schiros, K. S. Kim, H. Zhou, C. Gutiérrez, S. P. Chockalingam, C. J. Arguello, L. Pálová, D. Nordlund, M. S. Hybertsen, D. R. Reichman, T. F. Heinz, P. Kim, A. Pinczuk, G. W. Flynn and A. N. Pasupathy, *Science*, 2011, **333**, 999–1004.
- [24] F. J. Giessibl, *Reviews of modern Physics*, 2003, **75**, year.
- [25] Julian Chen, C, *Introduction to Scanning Tunneling Microscopy*, Oxford Science Publication, 2008.
- [26] J. E. Sader and S. P. Jarvis, *Applied Physics Letters*, 2004, **84**, 1801.
- [27] S. Hembacher, F. Giessibl and J. Mannhart, *Applied Surface Science*, 2002, **188**, 445–449.
- [28] A. A. F. K. S. Novoselov, A. K. Geim, S. V. Morozov, D. Tang, Y. Zhang, S. V. Dubonos, I. V. Grigorieva, *Science*, 2004, **306**, 666–669.
- [29] L. Gao, J. R. Guest and N. P. Guisinger, *Nano letters*, 2010, **10**, 3512–6.
- [30] M. Telychko, P. Mutombo, M. Ondráček, P. Hapala, F. C. Bocquet, J. Kolorenč, M. Vondráček, P. Jelínek and M. Švec, *ACS nano*, 2014, **8**, 7318–24.
- [31] D. Wei, Y. Liu, Y. Wang, H. Zhang, L. Huang and G. Yu, *Nano letters*, 2009, **9**, 1752–8.
- [32] A. Zabet-khosousi, L. Zhao, L. Pa, M. S. Hybertsen, D. R. Reichman, A. N. Pasupathy and G. W. Flynn, *Journal of the American Chemical Society*, 2014, 1391–1397.
- [33] C. Busse, P. Lazić, R. Djemour, J. Coraux, T. Gerber, N. Atodiresoi, V. Caciuc, R. Brako, A. T. N'Diaye, S. Blügel, J. Zegenhagen and T. Michely, *Physical Review Letters*, 2011, **107**, 036101.
- [34] A. T N'Diaye, M. Engler, C. Busse, D. Wall, N. Buckanie, F.-J. Meyer zu Heringdorf, R. van Gastel, B. Poelsema and T. Michely, *New Journal of Physics*, 2009, **11**, 023006.
- [35] M. P. Boneschanscher, J. van der Lit, Z. Sun, I. Swart, P. Liljeroth and D. Vanmaekelbergh, *ACS nano*, 2012, **6**, 10216–21.
- [36] P. Hapala, G. Kichin, C. Wagner, F. S. Tautz, R. Temirov and P. Jelínek, *Physical Review B*, 2014, **90**, 085421.

Appendices

Appendix A

Positions in the Moiré unit cell

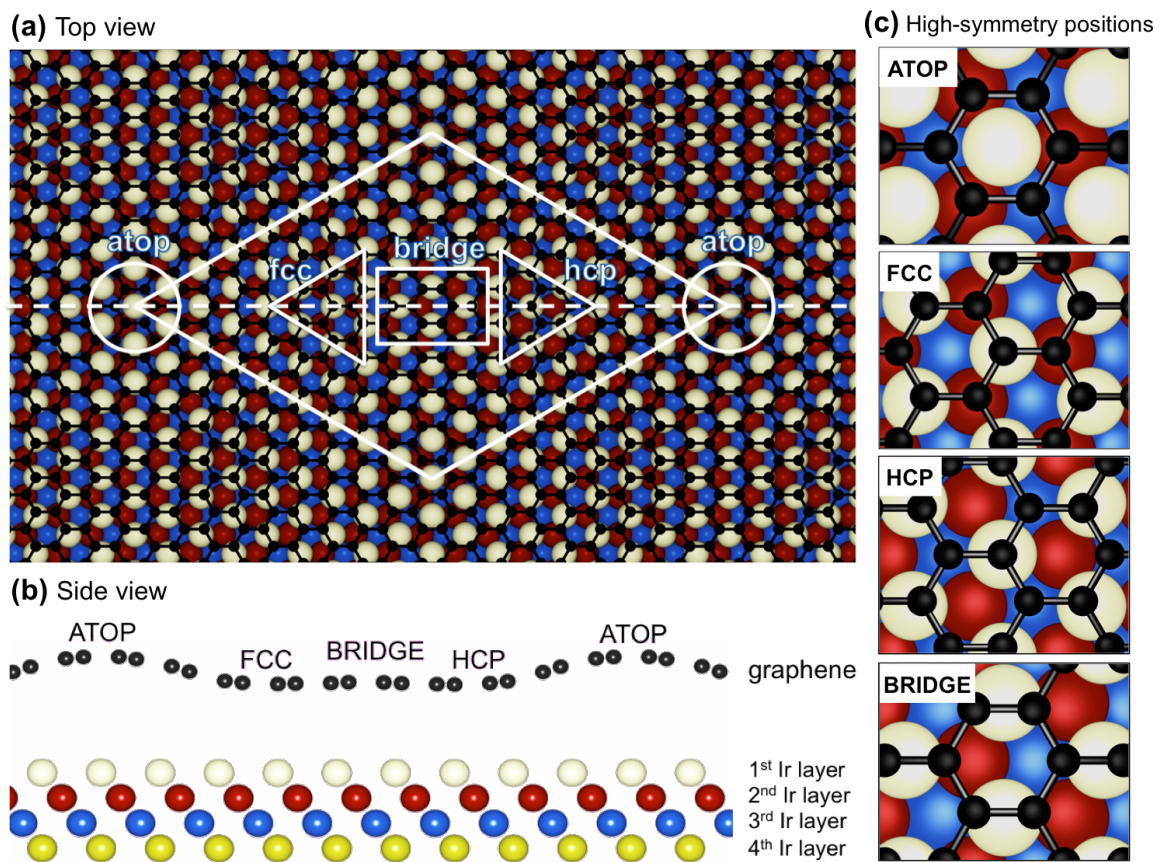


Figure A.1: An overview of all the high symmetry features that can be distinguished in graphene on an Ir surface (results are similar for other 6-fold symmetric substrates). (a) A top view of the Moiré unit cell is seen with all the distinct features marked. (b) A sideview with the height corrugation somewhat exaggerated to make it for clarity. (c) A zoom of the key features with the relative orientation with the underlying substrate. FCC and HCP sites are called valley sites throughout this thesis. Figure courtesy of G. Calogero. [22]

Appendix B

Results of a different N-dopant on Cu(111)

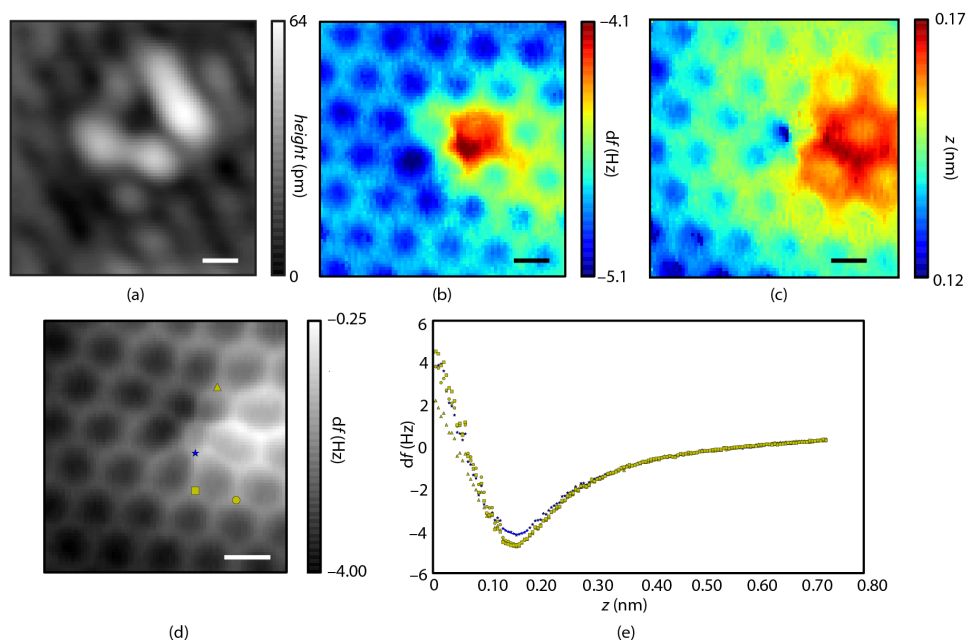


Figure B.1: (a) STM image of the N-dopant. (b) df -map. A map of the well depth on every pixel. (c) z -map. A map of the z -axis position of the well. (d) A constant height AFM image taken from the stack. The markers indicated positions on which individual spectra are taken. (a-d) Scalebars corresponds to 2.5 \AA . (e) The spectra belonging to the positions of the markers. The solid lines are the parabolic fits.

Appendix C

Chemical identification according to DFT

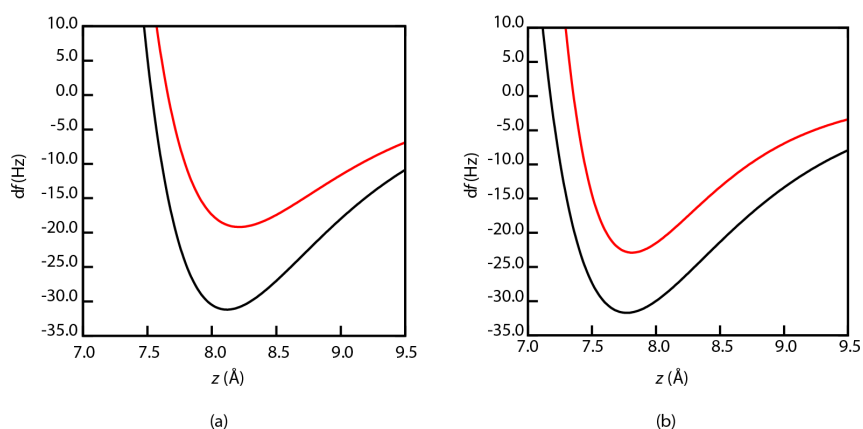


Figure C.1: Simulated $df(z)$ -spectra of a N atom and a C atom in (a) a top position and (b) a valley position. (a-b) The red spectrum stands for the N atom and the black for the C atom. As a tip model a tetrahedral tip consisting of four Ir atoms is used. These spectra were obtained by placing the tip exactly above the probed atom and by calculating the energies, at different tip-probed atom heights. This results in a LJ or Morse potential. By applying $F = \frac{\partial V}{\partial z}$ and equation 2.4 the $df(z)$ -spectra are found. During these mainly static calculations only the tip apex atom and the probed atom as well as its three neighbours were allowed to undergo a structural relaxation. The rest of the atoms in the cell were fixed at their relaxed positions with the tip infinity far away. These calculations were done using the Vienna Ab-initio Simulation Package (VASP) code.

